EAI Endorsed Transactions
on Pervasive Health and Technology
Research Article EAI.EU

Study on artificial intelligence recognition pre-processing algorithm for cervical cancer

Bo Feng[1,2], Chao Xu[1,2*], Zhengping Li[1,2], Jusheng Li[3], and Chuanyi Zhang[4]

[1]School of Integrated Circuits, Anhui University, Hefei, Anhui, 230601, China
[2] Engineering Laboratory of Agro-Ecological Big Data, Hefei, Anhui, 230601, China
[3]Nanjing University of Information Science & Technology, Nanjing, Jiangsu, 210044, China
[4]Department of Obstetrics and Gynecology, People's Hospital of Fanchang District, Wuhu, Anhui, 241000, China

Abstract

INTRODUCTION: Cervical cancer is the most common malignant tumor in the female reproductive system, with the number of deaths due to cervical cancer in developing countries accounting for 80% of the global total. In China, the incidence rate of cervical cancer is increasing year by year. At present, the commonly used methods for cervical cancer screening include TCT, HPV testing, TCT+HPV combined testing, FRD, and VIA/VILI. Among them, although TCT+HPV combined testing has high sensitivity and specificity, it is costly and time-consuming. VIA/VILI screening is cost-effective, easy to operate, and suitable for promotion in economically underdeveloped areas.However, VIA/VILI screening relies on the subjective judgment of doctors, so its accuracy is relatively low in rural areas of China with a large population and a lack of well-trained doctors. To address this issue, computer-aided diagnosis (CAD) technology is needed to improve the accuracy and reliability of VIA/VILI screening.
OBJECTIVES: The implementation of artificial intelligence (AI)-based Visual Inspection with Acetic acid (VIA) screening and computer-aided diagnosis has the potential to significantly reduce the cost of cervical cancer screenings and increase the coverage rate of cervical cancer screenings, thus reducing the incidence rate of the disease. To this end, we have developed an AI preprocessing algorithm aimed at improving the accuracy of AI in detecting cervical cancer.
METHODS: Initially, the algorithm maps images to the YCrCb and Lab color spaces. Unlike traditional enhancement methods that mainly focus on the luminance channel, our method primarily enhances the Cr channel in the YCrCb color space and a channel in the Lab color space. This paper innovatively proposes the LT_CLAHE algorithm to enhance the Cr channel, obtaining an enhanced image with a bias towards blue-green colors, and uses the WLS algorithm to enhance the a channel, obtaining an enhanced image with a bias towards red colors. Subsequently, the enhanced images from both color spaces are fused to eliminate color distortion.
RESULTS: Experimental results show that our method significantly enhances the texture of lesions and outperforms traditional methods across various objective indicators. When the enhanced images from this paper are used as input for neural networks, there is also a significant increase in the accuracy of neural network detection.

Keywords: Cervical Intraepithelial Neoplasia, Image Enhancement, Neural Network Pre-Processing, Contrast Limited Adaptive Histogram Equalization (CLAHE)

Received on 10 July 2024, accepted on 29 October 2024, published on 04 November 2024

doi:10.4108/eetpht.10.7724

1. Introduction

Cervical cancer incidence holds the top position among malignant tumors in the female reproductive system. According to data from the World Health Organization (WHO), there are 530,000 new cases [1]. Among these, the number of women dying of cervical cancer in developing countries accounts for 80% of the global number. In China, cervical cancer incidence is increasing year by year [2].

*Corresponding author. Email: shanlan578187814@126.com

Currently, the prevalent methods for cervical cancer screening are Thin Prep Cytologic Test (TCT), human papillomavirus (HPV), TCT + HPV, FRD, and Acetic Acid and Lugol's Iodine (VIA、VILI). TCT+HPV has high sensitivity and specificity, but is more expensive and time-consuming [3,4]. Folate receptor-mediated (FRD) screening is simple and inexpensive to perform, but it can only detect the presence of cervical disease and is difficult to determine specific kind of cervical disease. VIA/VILI has advantages such as being cost-effective, easy to operate, and offering timely diagnosis. It can be as effective as cytology for cervical cancer screening in economically undeveloped areas [5-9]. In other words, VIA/VILI screening is suitable for promotion in rural areas in China [10].

VIA/VILI screening is conducted by applying 5% white acetic acid solution to the surface of the patient's cervix, followed by observing the color of the patient's cervix under colposcopy [10]. Since VIA/VILI relies heavily on subjective experience and judgment of physician, the accuracy of VIA/VILI screening is relatively low in economically underdeveloped areas of China due to large population and lack of trained colposcopists [11]. Underwood et al. [12] reported an average positive colposcopy biopsy rate of 63.3%. To tackle this screening challenge, urgency is required for computer-aided diagnosis (CAD) enhancement to improve the accuracy and reliability of VIA/VILI screening.

However, identifying cervical cancer using neural networks is challenging because cervical intraepithelial neoplasia grade 1 and grade 2 (CIN1/CIN2) have only faint pale white lesion features [10], which are subtle and difficult to extract. Popular networks such as U-net, resUnet, transformer, GCN, and DenseNet are unable to capture the lesion features effectively for AI recognition. It has been reported [13] that, neural networks have been applied to identify cervical intraepithelial neoplasia, but the recognition results have no reference value as these papers used fewer than 500 samples for training.

Yuexiang Li [14] et al. proposed "Computer-Aided Cervical Cancer Diagnosis Using Time-Lapsed Colposcopic Images," in which AI identification was achieved by obtaining lesion characteristics of cervical intraepithelial neoplasia through differences in 5 cervical images taken at 30-second intervals after applying acetic acid. However, this method requires a colposcope with filters, which is expensive and not feasible for promotion in economically undeveloped areas. Additionally, delaying the photograph 5 times drastically alters the original operating procedure and habits of the physician. Consequently, physicians have demonstrated significant resistance to the method, both during the data collection phase and clinical trials.

A survey of 147 gynecologists knowledgeable about computer-aided diagnosis (CAD) revealed a general desire for an image enhancement technique that can enhance the textural features of CIN1 captured by colposcopy. It is hoped that this image enhancement technique will facilitate the physician's visualization and improve the accuracy of the neural network in identifying lesions without altering the original procedure.

In Figure 1, it can be observed that, the color of lesion texture and background are very similar, and the boundary of the texture is also blurred. Therefore, the core idea of image enhancement is 1) to increase the color difference between the texture and background without obviously changing its color, and 2) to make the boundary of the texture clearer.

(**a**) (**b**) (**c**)

Figure 1. ALow grade cervical intraepithelial neoplasia sample,(a) CIN2, (b) CIN1,(c) CIN2.

Current image enhancement techniques primarily involve a series of improved algorithms based on theories of histogram equalization (HE), Retinex, gamma correction (GC), dark channel, wavelet and transform, among others. Retinex can obtain a balance among dynamic range compression, edge enhancement, and color constancy, followed by development of single-scale Retinex (SSR) and multi-scale Retinex (MSR) algorithms [15], and multi-scale Retinex (MSRCR) [16] algorithm with color recovery. However, its poor performance in color stretching does not meet the requirements of this paper. Palanisamy et al. [16] proposed an enhancement method based on gamma correction and singular value decomposition, effectively highlighting blood vessel details in dark regions of the image. Zhou et al. [17] suggested a contrast enhancement method combining gamma correction and histogram equalization, which can emphasize blood vessels in fundus images, but has limitations in improving edge details in brighter image areas. Colposcopic images generally exhibit good illumination, and edge enhancement but this method is not significant. He et al. [18] proposed a dark channel prior algorithm for recovering high-quality fog-free images, which is unsuitable, as it weakens the texture features of pale white. However, this method is also unsuitable, as the detail layer decomposed by wavelet transform cannot effectively extract the texture of cervical precancerous lesions with colors close to background. Histogram equalization (HE) [19], which is simple and concise to implement, is widely used for contrast enhancement. However, processed images may have issues such as information loss, noise amplification, and excessive brightness enhancement. To address these problems, researchers have made numerous improvements based on HE [20], dualistic sub-image histogram equalization

(DSIHE) [21], and contrast-limited adaptive histogram equalization (CLAHE) [22].

Remarkable advancements in AI-driven image enhancement have been made recently. For instance, Li Y [14] introduced a deep auto-encoder to improve images without excessively amplifying features. Retinex-Net incorporated Retinex theory into CNN and devised a decomposition network capable of breaking down reflection and illumination components. These components were then combined with a correction module to enhance low-light images. Nonetheless, these existing algorithms remain insufficient for enhancing low-grade cervical precancerous lesions.

To significantly improve the textural features of CIN1 captured by colposcopy, an AI recognition pre-processing algorithm for cervical cancer was proposed. This algorithm substantially increases the color contrast between the lesion's texture and background without considerably altering the image color, while also making the lesion's outline more distinct. The primary innovations of our study are as follows:

(1) We propose an innovative approach to enhance lesion texture by enhancing color channels in the color space. This method ensures visual comfort while making the lesion texture more prominent.

(2) Enhancing color channels will inevitably cause color distortion in images, so a single-color space is insufficient to meet the requirements. To solve this problem, this study chooses Lab and YCrCb, two color spaces that complement each other. The images are decomposed into Lab and YCrCb color spaces, and enhancement is done separately on each color space to increase the color difference between lesion texture and background, and then the color distortion is removed by merging the two color spaces.

(3) This study proposes an innovative approach for enhancing contrast-limited adaptive histogram equalization, which is locally truncated, and enhancing the blue and green components in the YCrCb color space in a directional manner. An innovative approach is also proposed to enhance the red component of the Lab color channel in a directional manner by enhancing the detail layer of the A channel.

(4) The cervical intraepithelial neoplasia dataset PCC5000 was created, consisting of 5000 images of the cervix after acetic acid spraying, labeled by gynecologists.

2. Materials and Methods

2.1 Data Source

This paper involved the organization and classification of images on three publicly available datasets: the Microsoft Cervical Cancer Image Dataset [41], Google Cervical Cancer Segmentation[42], and Kaggle Cervical Cancer Image Classification[43]. From these, we acquired 2,000 colposcopic images exhibiting acetic acid whitening reactions of the cervix. The collection includes 510 samples of non-cervical intraepithelial neoplasia, 556 samples of CIN1, 513 samples of CIN2, and 421 samples of CIN3.The curated data have been named PCC2K.

2.2 Proposed Methods

AWhite acetic acid solution was applied to the surface of patient's cervix to detect abnormalities in the cervical area based on color changes and the shade of these changes. Pale white lesions at the patient's cervical squamous epithelial junction or outside the junction indicate CIN1, while thick white lesions in the patient's cervix with one side always at the squamous-columnar epithelial junction and distinct borders indicate CIN2. A thick, white, brittle mass with an irregular surface at the patient's cervix indicates cervical carcinogenesis.

CIN1, with its light and pale pinkish-white texture, is difficult to observe with naked eye and to recognize by a computer. Most image enhancement techniques enhance texture by altering the brightness and contrast of images. However, colposcopic images of the cervix are well-lit and high-resolution, meaning they cannot be enhanced by changing image brightness and contrast. Furthermore, since the texture of cervix itself is close in color to the texture of the lesion, enhancing the high-frequency component of the image is also not a viable method to improve the texture of the lesion.

Traditional image enhancement algorithms enhance the brightness channel in various color spaces [16-18]. However, in medical image enhancement, enhancing the brightness channel is limited in order to ensure visual comfort. Over-enhancement of the brightness channel can excessively enlarge the texture and background gradient, causing the image to appear unnatural and accelerating visual fatigue.

Color channel enhancement inevitably brings color distortion to the image, so a single-color space cannot meet the requirements. To solve this problem, this study chooses Lab and YCrCb color spaces, as shown in Figure 2. The image is decomposed into Lab and YCrCb color spaces, and enhancements are performed separately on these two-color spaces to enlarge the color difference between lesion texture and background. This study proposes an innovative method for locally truncated contrast adaptive histogram equalization, directional enhancement of blue and green components in the YCrCb color space, and directional enhancement of the red component in the Lab color channel using an innovative method of enhancing the detail layer in the A channel. These enhancements are then fused together to remove color distortion.

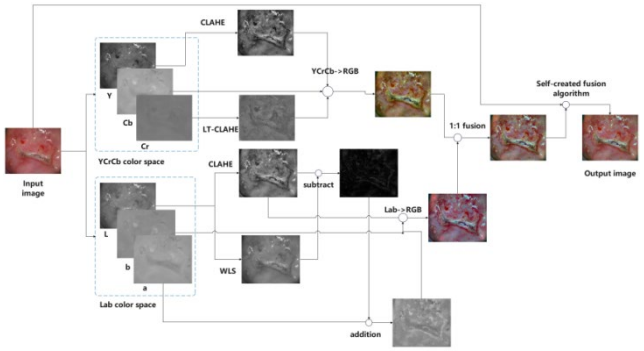

Figure 2. Algorithm flowchart, LT_CLAHE is local truncation limiting contrast histogram equalization

2.3 Absorption Characteristics of Lesion Texture Under Different Wavelength Illuminations

The surfaces of human organs such as the oral cavity, esophagus, stomach, vagina, and urethra consist of mucous tissue, which is mainly composed of an epithelial layer ranging from 100 μm to 500 μm and a mucous layer of approximately 1.5 mm [23]. Blood vessels are primarily distributed in the mucous and submucous layers. It is well known that the penetration ability of white light at each wavelength increases with increasing wavelength. The absorption properties of the epithelial layer, mucosa, and hemoglobin to the spectrum [23] are shown in Figure 1.

Figure 3 illustrates that the reflection coefficient of red wavelengths (600-650 nm) is significantly smaller in comparison to those of blue and green wavelengths. The penetration capability of red wavelengths is superior, enabling them to reach the submucous layer, whereas blue and green wavelengths are limited to the mucous layer, as they can be reflected by the mucosa and blood vessels. The vertical coordinates of Figures 3A&B are much smaller than those of Figure 3C, with hemoglobin demonstrating a superior reflection of blue and green wavelengths compared to the mucous and epithelial layers. Furthermore, the reflection of hemoglobin reaches its peak in the blue (415 nm) and green (540 nm) wavelengths. In summary, the green and blue components of colposcopic images offer microvascular information about the mucous layer, while the red component provides more extensive information regarding the submucous layer.

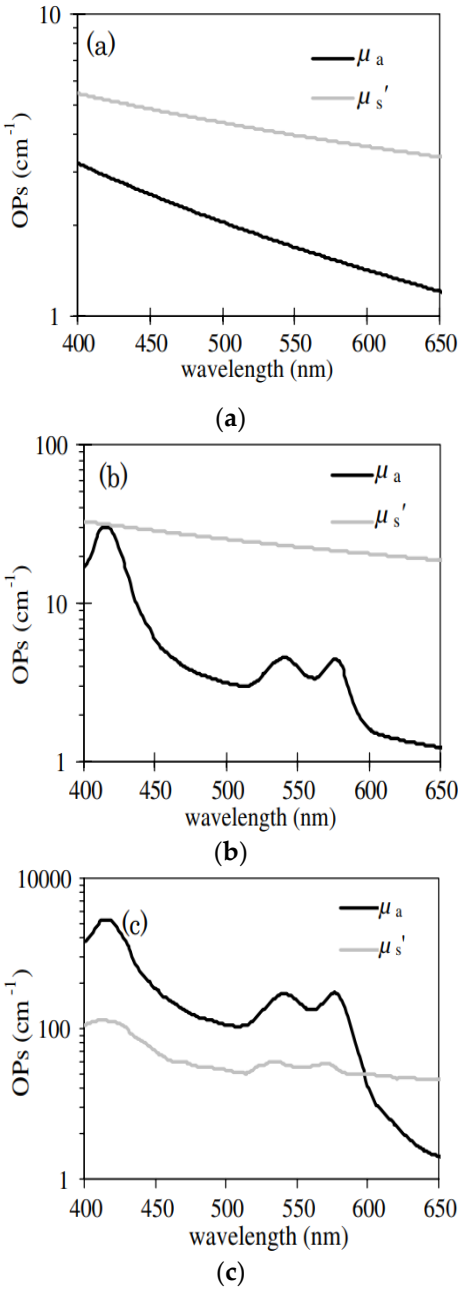

Figure 3. Absorption coefficient (μa) and reduced scattering coefficient (μ's) of (a) epithelium, (b) mucosa, and (c) oxygenated human blood

Cervical intraepithelial neoplasia can be observed progressing from the dermis upwards, eventually covering the entire mucous layer. Consequently, the blue and green components of the image yield more textural information pertaining to the lesion, whereas the red component presents less texture information about the lesion.

The cervical intraepithelial neoplasia develops from basement membrane of the mucosal layer and progresses upwards, covering the entire mucosal layer. Consequently, the penetrating ability of white light increases with wavelength, with red light reaching the basement membrane

and blue and green light being reflected by the lesion cells. Hence, the blue and green color components in the image contain more information regarding the lesion texture, while the red component has less information regarding the lesion texture.

The textural information in the R channel of the RGB color space appears very blurry in Figure 4, while the texture is relatively richer in the G and B channels. To enhance the contrast between the textural and background colors of the lesion, we heightened the weight of blue and green in the image.

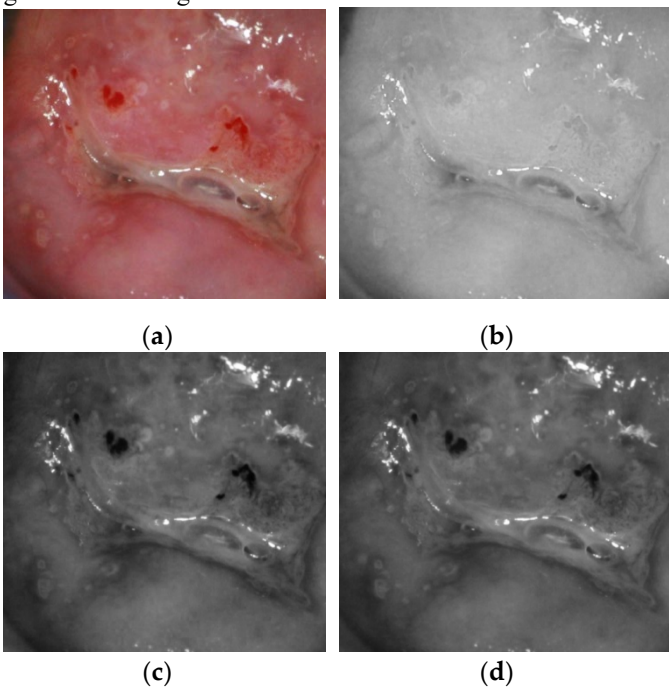

Figure 4. RGB color space:(a) original image; (b) R-channel; (c) G-channel;(d)B-channel;

2.4 Choosing appropriate color space

If we simply enhance the G and B components in RGB color space, it will alter the color of entire image and cause obvious distortion. Enhancing the color channels in any single-color space will result in significant color distortion. To address this issue, the image was converted to Lab color space and YCrCb color space, both of which consist of one luminance channel and two-color channels. The luminance channel and two-color channels operate independently of each other, as do the two-color channels themselves. This independence allows for increased blue and green weight without causing excessive distortion to the image.

In the Lab color space, L holds values ranging from 0-100 (pure black - pure white), where a ranges values between +127-128 (magenta - green), and b takes on values from +127-128 (yellow - blue).

We can easily observe that, blue and green are mainly distributed in second and third quadrants in the YCrCb color space. By selectively enhancing the Cr channel, we enhanced the blue and green components in the image without affecting the distribution of other colors. Moreover, red is distributed in the first and second quadrants in the LAb color space. By selectively enhancing the A channel, we can enhance the red part of the image without affecting the distribution of other colors.

As the lesion grows from the basal membrane of the cervical mucosa upwards, more blue and green lights are reflected from the relatively normal cervical skin. By selectively enhancing the Cr channel in the YCrCb color space, we enlarged the color gradient between the lesion texture and normal cervical skin. However, this enhancement may result in an overall cool color bias in the image. To address this issue, we selectively enhanced A channel in LAb color space to create a warm color-biased image. Finally, we fused the two images to remove color distortion.

2.5 Enhancement of Brightness Channel

Since the texture that required enhancement appeared as light white, and both the L components in the Lab color space and Y component in the YCrCb color space represent luminance in the image, enhancing L component and Y component can improve light white texture feature. The most commonly employed method for medical image enhancement is CLAHE (contrast-limited adaptive histogram equalization). In this study, CLAHE was adopted to enhance L and Y components, and after several trials, it was discovered that, the image did not experience significant distortion when the clipLimit was set to 1.5, and the texture of the lesion was enhanced to a certain extent.

CLAHE can limit local contrast enhancement by constraining the height of the local histogram, which in turn restricts noise amplification and excessive local contrast enhancement. Initially, image was divided into sub-blocks and subjected to histogram "clipping" (Figure 1A, followed by histogram equalization for each sub-block (Figure 1B)). Lastly, each pixel was interpolated to obtain transformed gray value, thus achieving contrast-limited adaptive image enhancement [24].

2.6 Color Enhancement in YCrCb Color Space

Blue and green colors in the YCrCb color space are primarily distributed in the second and third quadrants. By selectively enhancing Cr channel, the blue and green components in the image can be enhanced while minimizing the impact on other color distributions. Enhancing the blue and green components can make the texture of the lesion more prominent. To achieve directional enhancement of the

Cr channel, we innovatively propose a locally clipped contrast-limited adaptive histogram equalization method.

2.7 Local Truncated Contrast-Limited Adaptive Histogram Equalization (LT_CLAHE)

Traditional CLAHE reallocates the pixel points of each sub-block by evenly distributing the number of clipped pixels to each gray level of the histogram. Consequently, traditional CLAHE can enhance all colors evenly in the Lab and YCrCb color spaces. However, this enhancement effect is not very prominent since the lesion's texture is close to the background color. To address this issue, a local truncated contrast-limited adaptive histogram equalization is proposed in this study. The most innovative aspect of the method presented in this paper is introduction of an adaptive truncation value D, which determines the dynamic range of the final allocation, as the clipped pixels are no longer uniformly allocated.

The specific steps are as follows:

Step 1: Blocking. The input image was divided into non-overlapping sub-blocks of equal size, with M representing the number of pixels in each sub-block. Larger sub-blocks yield more noticeable enhancement effects but result in the loss of more image details

Step 2: Calculation of histogram. The histogram of sub-blocks is represented by h(x), with x representing the gray level, which falls within the range of [0, L-1], and L denoting possible gray levels.

Step3: Calculate the clipLimit with the formula:

$$\text{cliplimit} = \frac{M}{L} + \frac{(M - M/L)}{\text{normClipLimit}} \quad (1)$$

In which normClipLimit represents the contrast enhancement value, determining the magnitude of the contrast enhancement.

Step 4: Pixel point redistribution. For each sub-block, h(x) is clipped using the corresponding clipLimit value. Traditional CLAHE uniformly redistributes the clipped pixels to each gray level in the histogram. However, from Figure 4B, it can be observed that blue and green colors are mainly distributed in the lower part of the Cr channel. Therefore, the clipped pixels are redistributed between 0 and D as follows;

$$\text{totalE} = \sum_{x=0}^{L-1}(\max(h(x) - \text{clipLimit}, 0)) \quad (2)$$

$$\text{avgBIncr} = \frac{totalE}{D} \quad (3)$$

In the equation, totalE refers to the total number of pixel values exceeding clipLimit. avgBIncr refers to the average number of pixels increased per gray level in the histogram. The above allocation process is repeated until all clipped pixels are redistributed, If h'(x) denotes the histogram after pixel redistribution of h(x), where we have:

$$h'(x) = \begin{cases} h(x) & (x > D) \\ h(x) + avgBIncr & (x \le D) \end{cases} \quad (4)$$

In this formula, upperLimit = clipLimit — avgBIncr.

Step 5: Histogram equalization. Histogram equalization was performed on h'(x), with f(x) expressing the equalization result

Step 6: Reconstruction of pixel gray value. Based on f(x), the gray values for the central pixel points of each sub-block were obtained and used as a reference to calculate the gray values of each point in the output image by employing the bilinear interpolation technique,as shown in Figure 5.

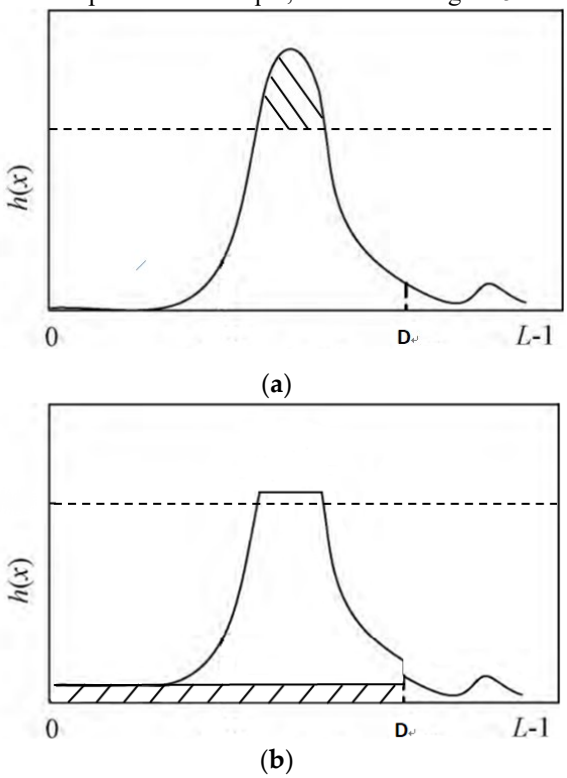

Figure 5. Local truncated contrast-limited adaptive histogram equalization;(a) Histogram before processing; (b) histogram after processing;

The precise truncation value D remains a topic for further exploration. If the value of D is too small, the blue-green color will be over-enhanced, causing significant color distortion. Conversely, if the value of D is too large, the enhancement will then be insufficient. A uniform D value for all images is also undesirable, as the color distribution of cervical images can vary widely depending on each physician's operating habits, colposcopic equipment, and the lesion. Furthermore, a uniform D value may cause some images to be over-enhanced and others to be under-enhanced. To address this issue, the study proposes adaptively obtaining the D value using the 3σ criterion.

$$D = \{x | \sum_{i=0}^{x} P(i) = T\} \quad (5)$$

Set probability density function as P (x)

$$P(x) = \frac{n_x}{N}(x = 0,1, \dots, L-1) \quad (6)$$

In this formula, represents the pixel number of xth gray level, N represents the total number of pixels in the digital image.

$$T = \sum_{i=0}^{\mu-\sigma} P(i) \quad (7)$$

The mathematical expectation and variance of the xth gray level of the probability density function P (x) was set as;

$$E(x) = \sum_{x=0}^{L-1} xP(x) \quad (8)$$

$$D(x) = E(x^2) - [E(x)]^2 \quad (9)$$

In the two formulas, μ and σ represent the expectation and standard deviation of the probability function P (x), respectively.

$$\mu = E(x)\ \sigma = \sqrt{D(x)} \quad (10)$$

2.8 Enhancement of Lab Color Space

We enhanced the A channel to create a warm-colored image in the Lab color space, which helps remove the distortion caused by YCrCb color space enhancement in the later fusion process. However, in this study, we did not continue to use the locally truncated contrast-limited adaptive histogram equalization for a channel enhancement. From the Figur4, it can be observed that, there is very little texture information in the red component, and small-scale enhancement will not enhance the texture, while large-scale enhancement will cause color distortion. To solve this problem, we first used the minimum mean square filter to extract the image details and texture from the L channel, and then fused the extracted details and texture with the A channel to obtain a warm-colored image.

2.9 Detail Extraction Based on Least Squares Filtering

The basic layer is obtained by applying weighted least squares filtering to structural layer, and the detail layer is obtained by subtracting the basic layer from the structural layer. Based on weighted least squares method, the detailed layer can extract good detail information while maintaining the original image structure, which is more effective for vaginal enhancement than artifacts and complexity in guided filtering and bilateral filtering.

Assuming the L channel is , and after CLAHE enhancement is.

WLS Model:

$$min_{l_{base}} \sum((u_p - g_p)^2 + \lambda(a_{x,p}(Lc_{structure})(\frac{\partial l_{base}}{\partial x})^2 + a_{y,p}(\frac{\partial Lc_{base}}{\partial y})^2)) \quad (11)$$

where p represents pixel point position, and ax and ay control the degree of smoothing at different positions. The first term represents that, the input and output images are as similar as possible. The second term is a common term that smooth the output image by minimizing the partial derivative. λ is used as a regularization parameter to balance two weights.

The detailed extraction model is as follows:

$$Lc_{detai}(x,y) = Lc_{structur}(x,y) - Lc_{base}(x,y) \quad (12)$$

2.10 Fusion of Detail Texture and A-channel

The fusion of detailed layer of L channel and A channel requires a suitable weighting factor α to enhance the A channel and highlight the lesion details. The weighted fusion model is given by:

$$Ae(x,y) = A(x,y) + \alpha Lc_{detai}(x,y) \quad (13)$$

$$\alpha = 0.1 + \frac{1+(std(A(x,y)))^{\frac{1}{2}}}{(std(Lc_{detai}(x,y)))^{\frac{1}{2}}+(std(A(x,y)))^{\frac{1}{2}}} \quad (14)$$

Std: standard deviation and : A-channel enhancement.

2.11 Image Fusion Algorithm

Enhancing the Cr channel in the YCrCb color space results in an overall cool color tone. On the other hand, enhancing A channel in Lab color space creates a warm color tone. Therefore, to address the issue of color shift, the enhanced images of the two-color spaces are fused in a 1:1 ratio.

The image in the Lab color space enhanced by the local truncated contrast-limited adaptive histogram equalization in this study is designated as IMG_LabE (i,j), and the image in the YCrCb color space enhanced by the local truncated contrast-limited adaptive histogram equalization in this study is designated as IMG_YCrCbE (i,j). Additionally, the original cervical cancer precancerous lesion image is designated as IMG(i,j), and the image after fusion is designated as IMG fuse (i,j).

$$IMG_{fuse}(i,j) = 0.5 \times IMG_{YCrCbE}(i,j) + 0.5 \times IMG_{LabE}(i,j) \quad (15)$$

The fused image no longer exhibits the defect of bluish or greenish color. The texture of the lesion is significantly enhanced, and color of the lesion area is also markedly different from that of the normal tissue. Transformer, ResUnet, and other commonly used neural networks for medical image recognition can effectively capture the features of the lesion in IMG_fuse (i,j). However, some doctors still consider the color of the fused image to be not soft enough, and a portion of the light-colored non-lesion tissues are over-enhanced, which is not favorable for doctors to observe and diagnose with naked eye. To address this issue, the original image IMG(i,j) is fused with IMG_fuse (i,j), aiming to retain the texture enhancement results for IMG_fuse (i,j) in the lesion area as much as possible, and increase the proportion of IMG(i,j) in the non-lesion area as much as possible.

According to the findings presented in literature [23], it is understood that normal cervical skin reflects more red light, while the lesion part contains a higher proportion of blue and green light.The image enhancement performed by the local truncated contrast-limited adaptive histogram equalization proposed in this study on Lab color space and YCrCb has minimized the effect on red component. Therefore, the color of non-lesion areas should not change much before and after enhancement, but the color of lesion

areas should exhibit a substantial change before and after enhancement.

In this study, 50 images of cervical precancerous lesions (including CIN1, CIN2, and CIN3) were randomly selected from the self-constructed PCC5000 dataset. Ten points were taken at each lesion area and non-lesion area for each image, and the coordinates of these points were recorded. Image enhancement was then performed on these 50 images of cervical cancer precancerous lesions using the aforementioned method, with 10 points being taken at each of the same locations. All the points were projected into HSV color space to compare changes in H-channel before and after enhancement. In HSV color space, H-channel contains color information in image.

The value of each point on the H-channel before enhancement is set as H1, and the value of each point on the H-channel after enhancement is set as H2, then

$$D\_value = |H1 - H2| \quad (16)$$

The distribution of the D_ value is shown in Figure 6, where it can be intuitively observed that the value change on the H-channel before and after enhancement in the non-focal region is very small, mostly below 10, while the value change on the H-channel before and after enhancement in the focal region is quite large. This observation provides a theoretical approach for fusion of IMG_fuse (i,j) and IMG(i,j). The smaller the change in value on the H-channel before and after enhancement, the higher the percentage of IMG(i,j). Conversely, the larger the change in value, the higher the percentage of IMG_fuse (i,j).

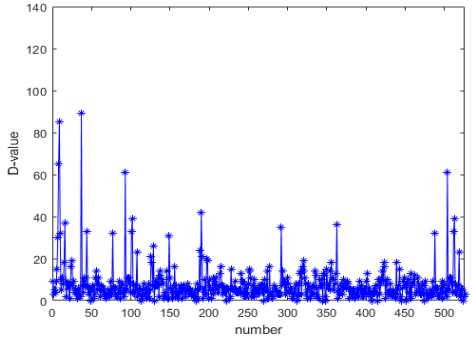

(a)

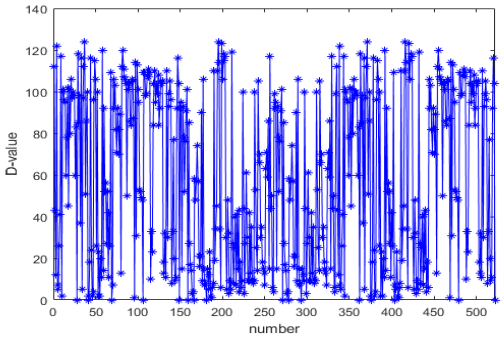

(b)

Figure 6. (a)D-value of non-lesional area;(a) D-value of lesional area.

Figure 6A reveals that, the number of values less than 15 in the non-focal area accounts for 69% of the total, and

values less than 30 account for 97% of the total. Based on the 3σ criterion, the following fusion equations can be derived:

$$\mathrm{IMG_{fuse2}(i,j)} = \begin{cases} A \times \mathrm{IMG(i,j)} + \mathrm{B} \times IMG_{fuse}(i,j), \mathrm{D\_value(i,j)} < 30 \\ 0.2 \times \mathrm{IMG(i,j)} + 0.8 \times IMG_{fuse}(i,j), \mathrm{D\_value(i,j)} \geq 30 \end{cases} \quad (17)$$

$$\mathrm{A} = \frac{[2 \times \mathrm{D\_value(i,j)} + 20]}{100} \quad (18)$$

$$\mathrm{B} = 1 - \mathrm{A} \quad (19)$$

$$D\_value(i,j) = |\mathrm{H1(i,j)} - \mathrm{H2(i,j)}| \quad (20)$$

3. Results and discussion

3.1 Comparison and Testing

In this section, a subjective and objective analysis of algorithms proposed in this study is presented, along with six classical image enhancement methods, including a series of improved algorithms based on theories of Retinex, Gamma Correction (GC), wavelets and transforms, and artificial intelligence. Classical neural networks such as Vision Transformer [25], densent [13], and convnext_tiny were also used to verify recognition accuracy of above neural networks, which was significantly improved after image enhancement of PCC5000 data using algorithms in this study. Test1 was in the CIN3 stage, Test2 was in the CIN2 stage, Test3 was in the CIN1 stage, Test4 was in the CIN2 stage, and Test5 was in the CIN1 stage.

As the texture of lesions in CIN1 is not very clear for observation with naked eye or recognition by a computer, the core requirement for image enhancement of this type is to enhance the lesion texture to facilitate naked-eye observation and AI recognition. Furthermore, to facilitate the physician's observation with naked eye, the image color should not be shifted too much, as it could interfere with physician's judgment of the disease,as shown in Figure 7.

The Multi-Scale Retinex (MSR) algorithm [15] leads to considerable distortion in the color of image without significantly enhancing the texture of the lesion. Multi-Scale Retinex with Color Restore (MSRCR) [26] can effectively enhance the texture of the lesion but at the expense of largely distorting the image color, making the image uncomfortable to view.

The algorithm proposed by Zhou et al. [17] effectively enhances the texture and blood vessels in the dark areas of the image. In Test1, it was observed that the brightness of the shadow part was significantly enhanced compared to the original image, and the texture of the shadow part was clearer. However, there was almost no enhancement of the lesion texture.

An Zhiheng's algorithm merges the benefits of Retinex-Net and wavelet transform to accomplish image enhancement, resulting in augmented texture of the lesion without significant color distortion. Nonetheless, the enhancement outcomes from Test 3 and Test 4 revealed that, the enhanced textures remained insufficiently clear.

The method proposed in this study demonstrates a notably superior enhancement of lesion texture compared to the other six approaches, maintaining overall color accuracy and providing a visually comfortable experience for subjective observation. This makes it highly suitable for gynecologists to perform diagnoses using the naked eye. Moreover, the lesion textures in the CIN1 stage during Test 3 and Test 5 experienced significant enhancement. However, this study's algorithm does not address illumination adjustments and fails to improve dark regions.

The acetic acid response map for cervical intraepithelial neoplasia indicates that, ample light is typically present at the cervix, where dark areas are virtually non-existent. Consequently, enhancing dark regions is deemed unnecessary within the context of this algorithm.

Objective metrics effectively assess quality attributes of enhanced images and quantitatively differentiate between superior and inferior image enhancement methods. Four reference evaluation indicators were selected:

The PCQI index [27] (Patch-based Contrast Quality Index) was devised as a flexible representation.

The Peak Signal-to-Noise Ratio (PSNR [28]) indicator serves to evaluate noise performance.

$$\mathrm{MSE} = \frac{1}{mn}\sum_{i=0}^{m-1}\sum_{j=0}^{n-1}[I(i,j) - K(i,j)]^2 \quad (17)$$

$$\mathrm{PNSR} = 10 \cdot log_{10}\left(\frac{MAXI^2}{MSE}\right) \quad (18)$$

where I and K symbolize the enhanced image and original image, respectively, MAXI denotes the maximum pixel value of the image, and MSE signifies the image's mean square error.

C_II [29] is a contrast assessment index tailored for medical images.

$$C\_\mathrm{II} = \frac{C_{processed}}{C_{original}} \quad (19)$$

$$C_{local} = \frac{max-min}{max+min} \quad (20)$$

where max and min represent maximum and minimum pixel intensity values in a window. Coriginal and

Cprocessed are the average of local contrast of image before and after processing, respectively.

The conventional image window size is set to 5 × 5 pixels. In other case, window size was set to 50 × 50 pixels for a more precise evaluation of endoscopic images [30].

The DV-BV [35] evaluation technique can segregate image pixels into background and foreground pixels. The BV value corresponds to the average of the variance of all background pixel neighborhoods, while the DV value denotes the average of the variance of all foreground pixel neighborhoods.

Table 1. Indicators processed by different methods

Method	Image	PCQI	PSNR	C_{II}	DV-BV
MSR	Test1	0.409	14.245	0.544	2.285
	Test2	0.590	15.455	0.701	5.129
	Test3	0.567	15.840	0.754	11.161
	Test4	0.554	15.292	0.646	1.956
	Test5	0.619	14.421	0.696	2.285
MSRCR	Test1	0.854	20.258	1.777	158.658
	Test2	0.988	19.984	1.986	29.687
	Test3	0.868	20.100	1.633	57.335
	Test4	0.857	19.088	1.884	8.585
	Test5	0.889	20.997	1.859	8245
Zhou	Test1	0.554	17.471	0.674	7.400
	Test2	0.803	21.576	0.904	10.860
	Test3	0.800	21.988	0.909	24.025
	Test4	0.768	21.483	0.922	2.903
	Test5	0.785	18.692	0.830	3.459
Tan W	Test1	0.569	23.295	0.952	9.042
	Test2	0.853	22.939	1.475	14.102
	Test3	0.819	21.279	1.476	32.873
	Test4	0.820	22.264	1.568	4.192
	Test5	0.845	23.295	0.952	9.042
retienx-net	Test1	0.437	14.008	0.520	2.149
	Test2	0.585	15.417	0.711	5.102
	Test3	0.549	15.799	0.727	11.080
	Test4	0.561	15.300	0.628	1.960
	Test5	0.602	14.315	0.599	2.185
	Test1	0.402	13.688	0.456	2.015
An Zhiheng	Test1	0.579	23.452	1.008	9.056
	Test2	0.901	23.012	1.511	14.154
	Test3	0.839	21.199	1.502	33.463
	Test4	0.888	22.789	1.597	4.628
	Test5	0.875	23.695	0.982	9.142
Ours	Test1	0.951	23.243	1.876	353.716
	Test2	1.086	22.674	2.086	34.017
	Test3	1.041	22.197	1.842	68.881
	Test4	1.062	22.059	1.944	10.905
	Test5	1.066	23.992	1.971	10.159

The algorithm presented in this study significantly outperforms other algorithms in terms of PCQI, C_II, and DV-BV, as shown in Table1. Moreover, it closely matches the algorithms proposed by Tan W and An Ziheng with regard to the PSNR index, surpassing other algorithms. The PCQI index in this algorithm is higher than in other algorithms, demonstrating improved image contrast and a clearer lesion texture. A higher PSNR value typically signifies better reconstructed image quality, and this study's algorithm also excels in the index. With a higher C_II index than other algorithms, this paper's algorithm proves its strength in the contrast evaluation index for medical images, suggesting that it can more effectively enhance the details of lesion texture. Furthermore, the algorithm surpasses other algorithms in the DV-BV index, which reflects the difference between background and texture. This indicates that, the algorithm can considerably magnify the disparity between focal and normal tissue, addressing the issue of lesions' texture and background color being too similar in the acetic acid staining map of cervical intraepithelial neoplasia.

3.2 Impact of Image Enhancement on Neural Network Accuracy in Identifying Cervical Intraepithelial Neoplasia

Experimental platform parameters were as follows: Windows 10 system, Intel i7-7700K, 4.02GHzx8, 32GB RAM, RTX3080Ti.

Three highly representative neural networks - Vision Transformer [25], Densenet [13], and Convnext_tiny - were chosen to verify the improvement of pre-processing algorithm on neural network accuracy in identifying cervical intraepithelial neoplasia. The PCC5000_Ours dataset was obtained after applying the image enhancement algorithm proposed in this study to all images in the PCC5000 dataset. The image enhancement algorithms proposed by Tan W and An Ziheng, as described in Sections 4.1 and 4.2, also exhibited some impact on the textural enhancement of cervical intraepithelial neoplasia. Their enhancement effects are significantly better than those of other comparison algorithms. Consequently, all images in the PCC5000 dataset were enhanced using algorithms proposed by Tan W and An Ziheng, resulting in the PCC5000_TanW dataset and PCC5000_AnZ dataset, which were used for comparative tests. Table 2 displays the accuracy of three neural networks in recognizing the four datasets.

Table 2. the accuracy of the three neural networks in recognizing the four datasets.

Dataset Name	Vision Transformer		densent		convnext_tiny	
	Accuracy (two categories)[1]	Accuracy (four categories)[2]	Accuracy (two categories)[1]	Accuracy (four categories)[2]	Accuracy (two categories)[1]	Accuracy (four categories)[2]
PCC5000	80.3%	68.2%	78.9%	60.6%	81.1%	62.8%

PCC5000_Ours	88.7%	79.2%	88.4%	73.8%	90.0%	71.7%
PCC5000_TanW	84.6%	71.8%	83.2%	68.6%	84.3%	66.4%
PCC5000_AnZ	85.9%	70.2%	81.7%	68.2%	82.9%	67.1%

Table 2 demonstrates that, the recognition accuracy of three neural networks in the binary classification case (where samples were divided into two categories: no lesion traces and lesion traces) improved after pre-processing with image enhancement algorithm presented in this study. This improvement was significantly greater than that of algorithms proposed by Tan W and An Ziheng. Additionally, in the case of quadruple classification (where samples were divided into no lesion traces, CIN1, CIN2, and CIN3), the recognition accuracy of all three neural networks substantially improved after pre-processing with this study's image enhancement algorithm. This is due to the clearer texture and more distinguishable features of each lesion cycle. However, the improvement of algorithms proposed by Tan W and An Ziheng in the case of quadruple classification was not as apparent.

3.3 Discussion on Novelty of Our Proposed Methods

The novelty of the proposed method is evident in the following aspects: An analysis was conducted on penetration ability of different wavelengths of light in the mucous layer and lesion development process for cervical intraepithelial neoplasia. This confirmed that, enhancing the blue and green color components can improve the texture of the lesion.

This study proposes a method for locally truncated contrast adaptive histogram equalization and directional enhancement of blue and green components in the YCrCb color space. Additionally, a technique for enhancing the red component in the Lab color channel is presented by increasing the detail layer in the A channel. Furthermore, a fusion algorithm is developed to remove color bias. This method significantly enhances the texture of lesions while maintaining comfortable observation by the human eye.

A local truncated contrast-limited adaptive histogram equalization with an adaptive truncation value D is thus herein innovatively proposed. Clipped pixels were no longer uniformly distributed, and instead, the dynamic range of final allocation was determined by the truncation value D, which was adaptively obtained with reference to the 3σ criterion in statistics.

4. Conclusion

In this study, a dual color space enhancement fusion algorithm was proposed to enhance the lesion texture by considering penetration ability of different wavelengths of light in the mucous layer and lesion development process for cervical intraepithelial neoplasia. Additionally, a local truncated contrast-limited adaptive histogram equalization was proposed to enhance blue and green components by utilizing the color distribution characteristics of Lab color space and YCrCb color space. Enhancement of red component was achieved by using a detail layer enhancement technique on A channel. Lastly, a custom image fusion algorithm was employed to remove color differences, providing a more comfortable visual experience while greatly enhancing the texture. The texture enhancement indicators in this algorithm outperformed those of other compared algorithms. As a pre-processing algorithm for neural networks, the algorithm proposed also significantly improves recognition accuracy and facilitates diagnosis by doctors using their naked eye.

Naturally, the algorithm proposed in this study has some limitations. For instance, a dedicated neural network recognition algorithm for cervical intraepithelial neoplasia was not proposed, and only three commonly used neural networks were applied to verify the recognition effect. In future research, the neural network will be improved based on Vision Transformer and will achieve a higher recognition accuracy by combining the pre-processing algorithm proposed in this paper.

Acknowledgements

This work was supported by the National Key Research and Development Program of China (No. 2019YFC0117800).

Ethical Compliance

This study was approved by the Ethics committee of School of Integrated Circuits, at Anhui University.

References

[1] Sung H, Ferlay J, Siegel R L, Laversanne M, Soerjomataram I, Jemal A and Bray F. Global Cancer Statistics 2020: GLOBOCAN Estimates of Incidence and Mortality Worldwide for 36 Cancers in 185 Countries. CA: A Cancer Journal for Clinicians 2021; 71(3):209-249.

[2] National Health Commission Of The People's Republic Of C.Chinese guidelines for diagnosis and treatment of cervical cancer 2018 (English version). Chinese Journal of Cancer Research Chung-Kuo Yen Cheng Yen Chiu 2019;31(2):295-305.

[3] Denny L, Kuhn L, De Souza M, Pollack A E, Dupree W and Wright T C. Screen-and-treat approaches for cervical cancer prevention in low-resource settings - A randomized controlled trial. Jama-Journal of the American Medical Association 2005;294(17):2173-2181.

[4] Jeronimo J.Secondary Prevention of Cervical Cancer: American Society of Clinical Oncology Resource-Stratified Clinical Practice Guideline Summary (vol 13, pg 129, 2017). Journal of Oncology Practice 2017; 13(7):466-466.

[5] Arbyn M, Sankaranarayanan R, Muwonge R, Keita N, Dolo A, Mbalawa C G, Nouhou H, Sakande B, Wesley R, Somanathan T, Sharma A, Shastri S and Basu P. Pooled analysis of the accuracy of five cervical cancer screening tests assessed in eleven studies in Africa and India. International Journal of Cancer 2008; 123(1):153-160.

[6] Bhatla N, Gulati A, Mathur S R, Rani S, Anand K, Muwonge R and Sankaranarayanan R. Evaluation of cervical screening in rural North India. International Journal of Gynecology & Obstetrics 2009; 105(2):145-149.

[7] Ferreccio C, Bratti M C, Sherman M E, Herrero R, Wacholder S, Hildesheim A, Burk R D, Hutchinson M, Alfaro M, Greenberg M D, Morales J, Rodriguez A C, Schussler J, Eklund C, Marshall G and Schiffman M.A comparison of single and combined visual, cytologic, and virologic tests as screening strategies in a region at high risk of cervical cancer. Cancer Epidemiology Biomarkers & Prevention 2003; 12(9):815-823.

[8] Qureshi S, Das V and Zahra F. Evaluation of visual inspection with acetic acid and Lugol's iodine as cervical cancer screening tools in a low-resource setting. Tropical Doctor 2010; 40(1):9-12.

[9] Sankaranarayanan R, Basu P, Wesley R S, Mahe C, Keita N, Mbalawa C C G, Sharma R, Dolo A, Shastri S S, Nacoulma M, Nayama M, Somanathan T, Lucas H, Muwonge R, Frappart L, Parkin D M and Cervic I M S G. Accuracy of visual screening for cervical neoplasia: Results from an IARC multicentre study in India and Africa. International Journal of Cancer 2004; 110(6):907-913.

[10] Poli U R, Bidinger P D and Gowrishankar S.Visual Inspection with Acetic Acid (VIA) Screening Program:7 Years Experience in Early Detection of Cervical Cancer and Pre-Cancers in Rural South India.Indian Journal of Community Medicine 2015; 40(3):203-207.

[11] Adsul P, Manjunath N, Srinivas V, Arun A and Madhivanan P. Implementing community-based cervical cancer screening programs using visual inspection with acetic acid in India:A systematic review. Cancer Epidemiology 2017; 49:161-174.

[12] Underwood M, Arbyn M, Parry-Smith W, De Bellis-Ayres S,Todd R, Redman C W E and Moss E. Accuracy of colposcopy-directed punch biopsies: a systematic review and meta-analysis.Bjog-an International Journal of Obstetrics and Gynaecology 2012; 119(11):1293-1301.

[13] Hu L M, Bell D, Antani S K, Xue Z Y, Yu K, Horning M P, Gachuhi N, Wilson B K, Jaiswal M S, Befano B, Long L R, Herrero R, Einstein M H, Burk R D, Demarco M, Gage J C, Rodriguez A C, Wentzensen N and Schiffman M. An Observational Study of Deep Learning and Automated Evaluation of Cervical Images for Cancer Screening. Jnci-Journal of the National Cancer Institute 2019; 111(9):923-932.

[14] Li Y X, Chen J W, Xue P, Tang C, Chang J, Chu C Y, Ma K, Li Q, Zheng Y F and Qiao Y L.Computer-Aided Cervical Cancer Diagnosis Using Time-Lapsed Colposcopic Images. IEEE Transactions on Medical Imaging 2020; 39(11):3403-3415.

[15] Zhang S, Wang T, Dong J Y and Yu H. Underwater image enhancement via extended multi-scale Retinex. Neurocomputing 2017; 245:1-9.

[16] Palanisamy G, Ponnusamy P and Gopi V P. An improved luminosity and contrast enhancement framework for feature preservation in color fundus images. Signal Image and Video Processing 2019; 13(4):719-726.

[17] Zhou M, Jin K, Wang S Z, Ye J and Qian D H. Color Retinal Image Enhancement Based on Luminosity and Contrast Adjustment. IEEE Transactions on Biomedical Engineering 2018; 65(3):521-527.

[18] He K M, Sun J and Tang X O. Single Image Haze Removal Using Dark Channel Prior. Ieee Transactions on Pattern Analysis and Machine Intelligence 2011;33(12):2341-2353.

[19] Jeong C B, Kim K G, Kim T S and Kim S K. Comparison of image enhancement methods for the effective diagnosis in successive whole-body bone scans. Journal of Digital Imaging 2011; 24(3):424-436.

[20] Ibrahim H, Kong N S P. Brightness preserving dynamic histogram equalization for image contrast enhancement. Ieee Transactions on Consumer Electronics 2007;53(4):1752-1758.

[21] Wang Y, Chen Q and Zhang B M.Image enhancement based on equal area dualistic sub-image histogram equalization method. Ieee Transactions on Consumer Electronics 1999; 45(1):68-75.

[22] Reza A M.Realization of the Contrast Limited Adaptive Histogram Equalization (CLAHE) for real-time image enhancement. Journal of Vlsi Signal Processing Systems for Signal Image and Video Technology 2004; 38(1):35-44.

[23] DuLe V N, Wang Q Z, Gould T, Ramella-Roman J C and Pfefer T J. Vascular contrast in narrow-band and white light imaging. Applied Optics 2014; 53(18):4061-4071.

[24] Pandey A K, Sharma P D, Dheer P, Parida G K, Goyal H, Patel C, Bal C and Kumar R. Investigating the Role of Global Histogram Equalization Technique for (99m)Technetium-Methylene diphosphonate Bone Scan Image Enhancement. Indian Journal of Nuclear Medicine 2017; 32(4):283-288.

[25] Castellanos M R, Szerszen A, Gundry S, Pirog E C, Maiman M, Rajupet S, Gomez J P, Davidov A, Debata P R, Banerjee P and Fata J E. Diagnostic imaging of cervical intraepithelial neoplasia based on hematoxylin and eosin fluorescence. Diagnostic Pathology 2015;10:119(1)-119(14).

[26] Jobson D J, Rahman Z U and Woodell G A.A multiscale retinex for bridging the gap between color images and the human observation of scenes. Ieee Transactions on Image Processing 1997; 6(7):965-976.

[27] Wang S Q, Ma K D, Yeganeh H, Wang Z and Lin W S. A Patch-Structure Representation Method for Quality Assessment of Contrast Changed Images. Ieee Signal Processing Letters 2015; 22(12):2387-2390.

[28] Rezazadeh S and Coulombe S. A novel discrete wavelet transform framework for full reference image quality assessment. Signal Image and Video Processing 2013; 7(3):559-573.

[29] Shin J and Park R H. Histogram-Based Locality-Preserving Contrast Enhancement. Ieee Signal Processing Letters 2015; 22(9):1293-1296.

[30] Xiong L, Li H Q and Xu L. An enhancement method for color retinal images based on image formation model. Computer Methods and Programs in Biomedicine 2017; 143:137-150.

[31] Wang S, Ma K, Yeganeh H, Wang Z, Lin W J. A patch-structure representation method for quality assessment of contrast changed images. IEEE Signal Process 2015;22:2387-2390.

[32] Rezazadeh S, Coulombe S. A novel discrete wavelet transform framework for full reference image quality assessment. Signal Image Video Process 2013; 7:559-573.

[33] Shin J,Park R-H J. Histogram-based locality-preserving contrast enhancement. IEEE Signal Process 2015;22:1293-1296.

[34] Xiong L, Li H, Xu L J. An enhancement method for color retinal images based on image formation model. Comput. Methods Programs Biomed 2017; 143:137-150.
[35] Ghimire D, Lee J. Nonlinear transfer function-based local approach for color image enhancement. IEEE Transactions on Consumer Electronics 2011;57(2): 858-865.
[36] Zhaohong Zhang, Wei Huang, Xiaoling Xue, Lanni Wang, Xiaoli Sun. Clinical Significance of the Special Stain for Epithelial Tissue in the Examination of Cervical Lesions by the Special Stain for the Uterine Cervix. Chinese Journal of the Frontiers of Medical Science (Electronic Version) 2014, 9: 4.
[37] Pretorius R G, Belinson J L. Re: An Observational Study of Deep Learning and Automated Evaluation of Cervical Images for Cancer Screening. Journal of the National Cancer Institute 2019; 112(10).
[38] Yasunari, Miyagi, Kazuhiro. Application of deep learning to the classification of uterine cervical squamous epithelial lesion from colposcopy images. Molecular and clinical oncology 2019; 11(6):583-589.
[39] Zhang T,Luo Y M ,Li P. Cervical precancerous lesions classification using pre-trained densely connected convolutional networks with colposcopy images. Biomedical signal processing and control 2020; 55(Jan.):101566.1-101566.11.
[40] Ying Z, Li G, Ren Y, Wang R, Wang W. A new image contrast enhancement algorithm using exposure fusion framework. In Proceedings of the International Conference on Computer Analysis of Images and Patterns, Ystad, Sweden, 22–24 August 2017; pp. 36–46.
[41] [Online].Available:https://github.com/microsoft/cervical-cancer-image-dataset
[42] [Online]. Available:https://github.com/google/cervical-cancer-segmentation
[43] [Online].Available:https://www.kaggle.com/datasets/kmader/cervical-cancer-image-classi